Revision based on time stamp, RR

Al diffusion in quartz

Nicholas D. Tailby[1,2,3*], Daniele J. Cherniak[2], E. Bruce Watson[2,3]

[1]*Department of Earth and Planetary Sciences, American Museum of Natural History, Central Park West at 79th Street, New York, NY 10024-5192.*

[2]*Department of Earth and Environmental Sciences, Science Center 1W19, Rensselaer Polytechnic Institute, 110 8th St., Troy, NY 12180, USA.*

[3]*New York Center for Astrobiology, Rensselaer Polytechnic Institute, 110 8th St., Troy, NY 12180, USA.*

Abstract

Aluminum diffusion in synthetic and natural quartz was characterized under anhydrous conditions at 1 atmosphere and temperatures from 700 to 950 ˚C. Experiments were carried out on polished quartz slabs immersed in fine-grained powder of spodumene or K-feldspar. Diffusion profiles were measured using Nuclear Reaction Analysis (NRA) and yield the following Arrhenius parameters:

D_{Al} (all orientations) = $2.48 \times 10^{-11} \exp(-199 \pm 10\ \mathrm{kJ.mol^{-1}}/RT)\mathrm{m^2s^{-1}}$, where $\log D_0 = -10.6 \pm 0.55$

The diffusivity of Al through the quartz lattice is sufficiently slow (e.g., akin to Ti) that diffusive modification or loss of Al in magmatic or metamorphic quartz is unlikely in all but the most extreme temperature-time conditions seen in natural systems. In other

words, core to rim Al zonation produced during crystal fractionation from a granitoid, or metamorphic overgrowths on quartz during metamorphism, are likely to be preserved at the crystal scale but may show some diffusive relaxation at the sub- to 10s of micron scale. The similar diffusivities of Al and Ti also suggest that diffusive modification of Al/Ti is highly unlikely to occur at all but the smallest length scales (e.g., sub- to 10s of microns). These observations indicate that the two most abundant impurities in quartz (Al and Ti) are likely to record primary information regarding the crystallization conditions in most geological environments.

Keywords: Quartz, diffusion, Al, Ti, trace element, granite, nuclear reaction analysis, Arrhenius parameters.

Corresponding author.
Phone: +1 212-313-7373
E-mail address: ntailby@amnh.org (N.D. Tailby)

Introduction

Quartz is arguably the defining mineral of the continental crust, and is found in a wide range of rock types, including the host metasediment of our planet's oldest materials (e.g., Jack Hills; Compston and Pidgeon, 1986). Recent studies have indicated that the concentration of some trace elements in quartz may be used as geochemical indicators (Ackerson et al., 2015). The Ti content of quartz, for example, has been linked to crystallization temperature and pressure (Wark and Watson, 2006; Thomas et al., 2012), and analyses reported from natural quartz have also been used to suggest that Al/Ti is a measure of melt fractionation (Müller et al., 2002; Jacamon and Larsen, 2009; Breiter et al., 2012, 2013). Trace element studies from a number of granitic bodies have also indicated that quartz Al content may be elevated in highly peraluminous melts (Jacoman and Larsen, 2009). These observations and hypotheses, combined with the fact that Al is often reported as the most abundant trace element to substitute within the quartz lattice (generally ranging from 10s to 1000s of ppmw; Götze, 2009), make constraining Al diffusion in quartz particularly pertinent.

The only study of Al diffusion to date is that of Pankrath and Flörke (1994), who used electron paramagnetic resonance (EPR) to determine kinetics and diffusivity within heat-treated natural grains (displaying notable Al zonation). This study, by contrast, reports measurement of Al diffusion through direct profiling methods, and results from experiments carried out on synthetic, initially Al-free quartz. Additional experiments were carried out on polished natural quartz grains from Arkansas and Herkimer (New York) to ensure natural grains display similar Arrhenius parameters.

In this study we report results from Al diffusion experiments carried out at 700-950 °C in order to define the Arrhenius parameters in quartz. Li profiling on selected samples is also employed to explore the possibility of coupling of Al and Li diffusion and the potential role of other coupled substitution mechanisms is considered as well. We also investigate the effects of crystallographic orientation on Al diffusion. The Al diffusion parameters obtained in this study are subsequently used to model Al diffusion within systems of comparable composition to those seen in granitic systems, both with and without Ti, and determine how diffusive processes may redistribute trace elements during cooling or thermal perturbations.

Methods

The majority of experiments were carried out on Al-free synthetic quartz (Westinghouse), though a number of experiments were also carried out on natural, gem quality quartz from Herkimer (New York) and Arkansas. The quartz crystals were cut into ~2x2 mm slabs with a low-speed wafering blade in two orientations – parallel and perpendicular to the c-axis. Crystal orientation was determined from crystal habit. The quartz slabs were polished with successively finer SiC grits (from 240 to 1500), finished with polishing in a 0.06 μm colloidal silica suspension, and cleaned ultrasonically in distilled water and ethanol. This lengthy preparation procedure ensures that the sample near-surface is free of defects attributable to the initial cutting and coarse polishing stages of preparation (Cherniak et al., 2014; Watson et al., 2016).

The experiments were conducted by the powder-source method (e.g., Watson and Dohmen, 2010) using two general types of source, both designed to accommodate coupled substitution of Al^{3+} on the quartz lattice. Exchange reactions possibly describing experiments presented here include:

$$LiAlSi_2O_6 = Li^+Al^{3+}O_2 + 2SiO_2 \quad (\textbf{\textit{eq. 1}})$$

Spodumene = *Quartz* + *Quartz*

and,

$$KAlSi_3O_8 = K^+Al^{3+}O_2 + 3SiO_2 \quad (\textbf{\textit{eq. 2}})$$

K-feldspar = *Quartz* + *Quartz*

and,

$$Al_2SiO_5 = Al_2^{3+}\square O_4 + SiO_2 \quad (\textbf{\textit{eq. 3}})$$

Kyanite = *2Quartz* + *Quartz*

Where, $\square$ denotes an oxygen vacancy.

A number of additional coupled substitution mechanisms have been hypothesized for Al-in-quartz (derived from both measurements of natural quartz and theoretical

determinations), and multiple coupled substitution mechanisms may occur in natural quartz. The dominant substitution mechanism for Al^{3+} is thought to involve monovalent cations, such as H^+, Li^+, Na^+ and K^+, (Botis and Pan, 2008), but in all cases Al^{3+} is likely the rate limiting species during diffusive exchange. Previous investigations of alkali diffusion in quartz have shown that the monovalent elements diffuse much faster than elements of higher charge (Cherniak, 2010), suggesting that Al^{3+} is likely to be the slowest species during diffusive exchange involving coupled substitutions. Two alkali elements of highly different ionic radius and previously reported diffusivities were employed in this study in order to investigate whether these influence the rate of Al^{3+} diffusion.

The first type of diffusant source used in the present study incorporates powders of spodumene ($LiAlSi_2O_6$) and K-feldspar ($KAlSi_3O_8$), synthesized from high-purity reagent grade oxide and carbonate powders (Alfa Aesar). Mixtures of Li_2CO_3-Al_2O_3-SiO_2 and K_2CO_3-Al_2O_3-SiO_2 were combined in stoichiometric proportions for spodumene and feldspar, respectively, ground under acetone in an agate mortar, heated slowly to 600 °C, and held at this temperature for 24 hours to drive off CO_2. The fired mineral powders were subsequently ground under acetone in an agate mortar and held at 200 ˚C in a drying oven prior to its use in diffusion experiments to ensure anhydrous conditions at the start of the experiments.

The second type of diffusion source powder incorporated natural spodumene, kyanite or oligoclase, ground under acetone in an agate mortar and fired at 600 ˚C prior to

experimental runs. Spodumene powder was sampled from the Strickland pegmatite (Connecticut), kyanite was sampled from Minas Gerais (Brazil) and oligoclase was obtained from Alfa Aesar. Like the synthetic source powders, the natural mineral powders were kept at 200 ˚C prior to experiments to ensure anhydrous conditions during diffusion anneals.

The powder-source experiments were assembled by placing the source material and pieces of polished quartz in a silica glass ampoules, which were sealed under vacuum (Figure 1). Prepared capsules were suspended in Kanthal-wound vertical tube furnaces, with temperatures monitored with type K (chromel-alumel) thermocouples positioned immediately adjacent to the capsules.

Table 1 outlines the temperature-time conditions for the experiments and demonstrates that run conditions ranged from 700-950 ˚C and 21 to 1440 hours. Following diffusion experiments and NRA analysis, all quartz sample surfaces were examined for evidence of surface reactions via electron imaging on a Cameca SX100 fitted with a LaB_6 crystal, housed at the Rensselaer Polytechnic Institute.

The synthetic and natural quartz crystals used in experiments were analyzed by LA-ICP-MS to ensure the starting material was essentially a blank (i.e., $X^{quartz}_{A^+Al^{3+}O_2} \approx 0$), where A^+ denotes an alkali or proton). Analyses of the synthetic Westinghouse quartz yield an Al content prior to experimentation of 2.7 ± 0.7 ppmw (LOD = 1.4 ppmw), while analyses of Herkimer and Arkansas quartz both yield Al concentrations below the limit of

detection. Information regarding quartz LA-ICP-MS analysis and a representative time-resolved ablation profile can be found in Supplement 1.

Analytical techniques

Nuclear Reaction Analysis (NRA) of Al and Li

Al concentration profiles in quartz samples were measured with nuclear reaction analysis (NRA) using the reaction $^{27}Al(p,\gamma)^{28}Si$. Li concentration profiles on selected samples using Li-bearing sources of diffusant were measured with NRA using the reaction $^{7}Li(p,\gamma)^{8}Be$. These analyses were performed at the Ion Beam Laboratory at the University at Albany, using proton beams produced by the Dynamitron accelerator. For Al profiling, the 992 keV resonance of the reaction was employed, with a bismuth germanate (BGO) detector used to detect gamma rays produced in the reaction (Cherniak, 1995; Cherniak and Watson, 1992). Typical beam current is 50-80 nA and the dose for each beam energy ranges from 20-40 μC. At these working conditions the typical detection limit is ~100 ppma, which is well below the concentrations of experiments presented here. Each Al depth profile is comprised of multiple analyses at a series of incident beam energies. Energy steps of 1.0 - 0.5 keV for the incident proton beam were taken near the resonance energy to profile Al at depths near the sample surface, with larger energy steps (2-5 keV) at greater depths (above ~150 nm). Spectra from untreated specimens of quartz were also recorded at each energy step to evaluate background levels in the gamma energy region of interest, and gamma spectra of Al foil were collected as a standard to convert gamma yields into Al concentrations for quartz samples. Depth scales for the Al profiles were

calculated from the energy difference between the incident proton beam and the resonance energy, and by the stopping power (energy loss of the protons as a function of depth in the material); stopping powers used in depth calculations determined with the software SRIM (Ziegler and Biersack, 2006).

Li profiling was conducted using the 441 keV resonance of the $^{7}Li(p,\gamma)^{8}Be$ reaction, with an approach similar to Cherniak and Watson (2010) and Trail et al. (2016). As with the Al profiling, Li depth profiles were obtained by varying beam energy to measure Li at greater depths in the sample. Energy steps of 1 keV were used at energies near the resonance energy, with energy steps increased to 3-5 keV at greater depth within the quartz. The gamma rays produced in the reaction were detected with a bismuth germanate detector. Specimens of spodumene were also analyzed as standards for determining Li concentrations, and for use in calibration of gamma energy spectra. Samples of untreated quartz were analyzed to evaluate background levels in the gamma energy region of interest. The depth scales were calculated from the difference between the incident beam energy and the resonance energy, which was divided by the energy loss per unit depth in quartz for protons of this energy range, as determined from the SRIM software (Ziegler and Biersack, 2006).

Results

Figure 2a (data and profile fit) and Figure 2b (two profiles from experiments at constant temperature at different time intervals) show typical Al diffusion profiles from quartz diffusion anneals, with diffusivity results reported in Table 1.

For experiments carried out parallel to the c axes (and incorporating the low T data of Pankrath and Flörke, 1994) we report an activation energy for Al diffusion of 198 ± 18 kJ/mol and a pre-exponential factor of 2.40 x 10^{-11} (log D_0 = -10.6 ± 0.67) from least squares fitting. Diffusion results from experiments perpendicular to the c axis (incorporating the low T data of Pankrath and Flörke, 1994) are very similar, yielding an activation energy of 200 ± 13 kJ/mol and a pre-exponential factor of 2.51 x 10^{-11} (log D_0 = -10.6 ± 0.66). These two datasets, graphed in Figure 4c, indicate there is little difference in diffusivity for the two orientations.

Calculations of Arrhenius parameters using the diffusion data for both orientations (including the low temperature data of Pankrath and Flörke, 1994) result in an activation energy of 199 ± 10 kJ/mol and a pre-exponential factor of 2.48 x 10^{-11} (log D_0 = -10.6 ± 0.55). This indicates a diffusivity similar to Ti, with slightly lower activation energy.

Li diffusion profiles on selected samples provide some insight into substitutional mechanisms for Al diffusion in quartz. In some of samples in which Li was profiled, Al and Li profiles are of similar length and concentration (Figure 3). However, there are cases in which Li profiles display complex shapes that differ from simple error functions, and other cases in which Li concentrations are significantly lower than those of Al. The

complex Li profile shapes may indicate that Li diffusion occurs on multiple sites, as observed in experiments on Li diffusion in olivine by Dohmen et al., 2010, where Li diffusion is hypothesized to occur on octahedral and interstitial sites, and is intimately related to vacancies. The correspondence of Li and Al profiles in some samples points to the potential for coupled Al-Li diffusion in quartz, but the similarity of Al diffusivities in samples using a variety of diffusant sources (with and without Li) indicates that Al is the rate-limiting species. Drawing broader conclusions regarding substitutional mechanisms for Al diffusion in quartz and potential complexities of Li diffusion is not warranted given the scope of this study.

Surface concentration

The use of a semi-infinite source material in a diffusion experiment has the advantage that surface concentration remains constant (independent of time) and defines equilibrium partitioning where source and crystal surface are equilibrated at experimental conditions. This being the case, measured surface concentration is also dependent on the spatial resolution and detection limits of the analytical method. It is important to evaluate whether surface concentrations measured in this study provide useful information regarding Al concentration. The time-series study carried out on identical experiments, where experiments were held at constant temperature using the same starting material (795 ˚C; see Fig. 2), show broadly similar surface concentration (see Table 1), despite experiment duration ranging between 10 and 48 days. This suggests that the surface

concentration described from experiments presented here are near-constant at the resolution of the NRA technique.

The calculated quartz surface concentration from experiments at different temperatures may also be considered. Recorded values range from ~1300 ppmw (700 ˚C) to ~4300 ppmw (950 ˚C), with an average of 2407 ± 806 ppmw over the entire temperature range (700-950 ˚C). These concentrations are in agreement with previous experimental work where quartz was synthesized in the presence of an Al_2SiO_5 polymorph, which shows an Al content of 1146 ± 64 ppmw at 10 kbar/900 ˚C and 534 ± 75 ppmw at 15 kbar/900 ˚C (Tailby et al., 2010). These collective datasets clearly indicate a notable pressure effect on Al-solubility in quartz, a result highly consistent with other cations known to substitute within the quartz lattice (e.g., Ti; Thomas et al., 2010). The Ti content of quartz equilibrated with rutile rapidly increases with decreasing crystallization pressure (at 900 ˚C); varying from 63 ppmw at 20 kbar, 103 ppmw at 15 kbar, 327 ppmw at 10 kbar and 813 ppmw at 5 kbar (>1000 % change in concentration). On the basis of these two datasets, which represent the two most abundant trace elements in quartz, it seems likely that quartz crystallized at atmospheric pressure (in the presence of an aluminous phase) contains high Al concentrations (e.g., >>1200 ppmw).

Analyses of Al content in natural quartz can also be found within the literature, with values reported from quartz at Jerritt Canyon and McLaughlin (3500 ppm; Rusk, 2008), and Mt Leyshon (1000 ppm; Allan and Yardley, 2007) reporting values in the thousands of ppmw. Although the high Al contents from hydrothermal quartz grains are not directly

comparable to experimental samples in the present work, it does demonstrate that comparable Al concentrations are seen in nature.

Discussion

Results presented in Table 1 and Figure 4 demonstrate that our Arrhenius parameters for Al diffusion are consistent with results reported by Pankrath and Flörke (1994), as their data fall on a down-temperature extrapolation of the Al diffusion relations determined in the present study, good agreement despite the employment of experimental methods, temperature-time conditions and analytical techniques that are significantly different across the two studies. Experimental results presented in this study also demonstrate that Al diffusivities are remarkably consistent among experiments using different diffusant sources – including natural and synthetic compounds of different composition. This indicates that Al diffusivity is insensitive to the charge-balancing alkali species involved in diffusion (i.e., ***eq. 1*** versus ***eq. 2*** versus ***eq. 3***), suggesting that Al is the rate limiting element for diffusion into quartz. This result is consistent with existing diffusion data for quartz (see Figure 4), which demonstrates that the monovalent species (e.g., alkali elements and protons) display much faster diffusivities than Al^{3+}. This is an important observation as a number of trace element studies in granitic systems report Al content in relation to potential charge-balancing species in quartz – H^+, Li^+, Na^+, K^+ (Breiter and Müller, 2004; Götze et al., 2004; Larsen et al., 2004; Müller et al., 2008; Landtwing et al., 2005). In order to determine whether these trace element signatures preserve quartz chemistry from the time of crystallization in a cooling granitoid, it is necessary to consider the relative diffusivities of these species. It may be possible to exchange Li^+ for

H^+ within quartz in the presence of a concentration gradient in a cooling magmatic quartz crystal (given the much faster diffusive rates of alkalis in quartz – see Figure 4); diffusive loss or relaxation of Al^{3+} is much less likely to occur over the same cooling interval.

Modeling Al diffusion during cooling.

Quartz crystals commonly exhibit heterogeneous distribution of Al and other trace impurities in the form of zoning acquired during growth. This zoning can be sectoral (Jourdan et al., 2009) or broadly oscillatory (Wiebe et al., 2007) in nature, and is generally attributable either to growth-related kinetic effects — growth entrapment (Lanzillo et al. 2014); diffusive boundary layer in the growth medium (Watson and Müller, 2009) — or to abruptly changing system conditions. The Arrhenius law for Al diffusion obtained in this study makes it possible to model relaxation of Al zoning for various initial distributions of Al and any imagined temperature-time (T-t) history. We used a finite-difference numerical approach similar to that described by Watson and Cherniak (2013) to model diffusion in a sphere over an arbitrary (linear) T-t path, but modified to accommodate non-uniform initial distributions of diffusant in the form of concentric spherical zones having different concentrations (these zones mimic oscillatory variations acquired during growth). The details of the numerical algorithm and its accuracy are described in Watson and Cherniak (2013). The approach is also similar to that implemented by Watson et al. (2010) for a cylindrical geometry, but we saw no added value in modeling a cylindrical shape in the present study because quartz crystals in igneous rocks are generally equiaxed, and because our new data indicate that the diffusivity of Al in quartz does not depend upon crystallographic direction.

A minor difference between the current modeling strategy and that followed by Watson and Cherniak (2013) is that the present investigation did not require especially close node spacing near the surface of the spherical crystal, which Watson and Cherniak used to accurately capture the diffusive flux at the surface for diminishingly small values of $D{\cdot}t$. In the present study, we used a fixed number of 500 radial nodes for all simulations. The main goal of the modeling was to evaluate the extent to which early-formed Al zonation in quartz crystals is preserved during protracted cooling. Another focus of this research was to investigate diffusion-controlled changes in elemental ratios of elements currently employed in geochemical studies on quartz (e.g., Al:Ti or Al:Li).

The initial temperature (T_0) for all quartz diffusion modeling was set at 700 ˚C or 650 ˚C, a temperature near or just below the granite solidus at 3 kbar and conditions at which significant quartz crystallization has likely occurred in a granitic system. To demonstrate the point, the Shannon's Flat granodiorite (Joyce, 1973) as modeled in MELTS at 3 kbar and NNO, reports ~84 % quartz crystallization (22 modal percent quartz, at 83 percent magma crystallization) by 700 ˚C.

Cooling rates estimated from closure temperatures in the Cooma granodiorite (Lachlan Fold Belt; Tetley, 1979) indicate a value of 15-20 ˚C/My. Cooling from ~700-300 ˚C in granitoids of the Murrumbidgee batholith (Lachlan Fold Belt, Roddick and Compston, 1976) was estimated to occur over ~4 My and suggests a cooling rate of ~100 ˚C/My. Cooling rates from the John Muir intrusive suite (Sierra Nevada; Davis et al., 2012)

report values of ~65 ˚C/My. Based on these estimates of cooling rates in different granitoids, diffusion models carried out here employed rates ranging from 0.1 to 100 ˚C/Myr over a 200 Myr time interval. 500 ˚C was selected as the model terminus, as diffusion at and below this temperature is negligible.

It should be stressed that diffusion models based on monotonic cooling represent only one scenario by which quartz trace element geochemistry may be modified in a cooling granitic system. Various phenomena may complicate cooling paths in magmatic systems, including incremental emplacements within an intrusive sequence that will radically change time-temperature paths in a cooling system. Similarly, post-crystallization deformation, recrystallization or dissolution-precipitation processes may dramatically change Al concentration. In short, the models presented here represent simplified systems in order to provide some evaluation of diffusive processes that can modify trace element composition and ratios in natural quartz grains.

Geological applications: results from models.

Four simulation strategies were used to evaluate the implications of diffusion results presented here for natural systems. The first method represents a simple diffusion model of an Al- zoned grain (2.5 mm in radius, Figure 5) as a function of time, temperature, cooling rate and Al domain thickness. The results from this model are presented in Figure 5 and provide a visual indication of how diffusion can modify preexisting Al concentration heterogeneities in quartz. These simulations clearly indicate that fairly small-scale (<10 μm domains) Al compositional domains in quartz show limited

diffusive relaxation (chemical homogenization) at moderate cooling rates seen in nature (e.g., 50-100 ˚C/Myr). Very fine-scale compositional domains (e.g., <5 µm domains) by contrast, such as those visualized via cathodoluminescence in volcanic grains, may potentially be modified by diffusion at much faster cooling rates (e.g., 100 ˚C/Myr). This is to say that there is some capacity for original zonation patterns within intrusive quartz-saturated magmas, to be "smeared" by diffusive processes in slow cooling magmas. This being the case, a 2:1 compositional spread (as used in the modeling) within a quartz grain is high compared with compositional ranges in natural systems, so it seems unlikely that diffusion will significantly modify quartz Al content.

The second modeling technique quantifies the amount of or percentage change within an individual, initially homogenous, domain within a zoned crystal. Figure 6 highlights how the model calculation is performed. In this example, we begin with a 5 mm spherical quartz grain having concentric spherical domains (shells) between which Al concentration varies by a factor of 2 (arbitrarily specified as 100 and 50 ppmw, but outcomes depend on the ratio, not actual values). It should be noted at this concentration ratio the maximum change possible within any individual domain is 25% of 2:1. The effect of domain width can be explored by changing the number of domains. Concentration ratios other than 2:1 would result in somewhat different intra-zonal % changes in Al concentration for a given thermal history, so the 2:1 choice should be considered as illustrative. Model results are reported in Figure 7, which reveals the critical dependence of percent change within a given domain is dependent on domain width (highlighting the importance of diffusive length scales).

The third modeling approach combines calculations incorporating time and cooling rates to determine when the geometric center of a domain within a zoned crystal changes by 0.1 %, in essence a center or core-retention calculation. The retention of domain-core Al content is an important consideration for the analysis of magmatic quartz, as it represents the point in time where a grain no longer records true magmatic Al-signature. It is worth noting that the value of 0.1 % is arbitrary, but was selected on the basis that most modern analytical methods can detect a 0.1 % change in concentration. Figure 8 provides a simple visualization of the conditions under which magmatic quartz of broadly similar size (e.g., radius of 2.5 mm) will preserve core Al concentration values. This shaded region in Figure 7 spans a broad time-cooling rate space within which little/no detectable change in quartz Al concentration will be detected. Interestingly, many cooling rates estimated from quartz-saturated granitoids likely fall within or just outside this "region of retention" even when domain size (width) is small. This, again, suggests that most magmatic quartz will preserve primary information regarding crystallization conditions (though some exceptions are possible). An example of this type of calculation can be seen in Figure 7b, where a quartz crystal with a radius of 2.5 mm and 500 µm concentric domains undergoes cooling at 60 ˚C/Myr (see vector b-b'). A quartz crystal along the b-b' cooling path will see progressive decrease in Al concentration from the domain (ranging from 0.0-5.4 % loss) but never loses core concentration regardless of time. In this scenario the core cooling rate-time curve never intercepts the core retention curve. The same crystal-domain size configuration cooling at 30 ˚C/Myr (see a-a') shows progressive domain loss (from 0.0-6.6 % loss) until ~1.15 Myr, when the core retention curve is

intercepted. At this point the crystal begins to lose "primary core concentration" such that analysis is likely to misrepresent initial Al content. This simple example demonstrates the important relationship between domain size, cooling rate and time for the preservation of primary quartz composition in zoned crystals.

The fourth and final modeling strategy combines diffusive parameters for Al and Ti, the two most abundant and readily studied trace elements in quartz, in order to determine how Al/Ti can be modified during cooling. The rationale behind this research is that Al/Ti has been hypothesized as a measure of melt fractionation in quartz-saturated systems in numerous studies (Müller et al., 2002; Jacamon and Larsen, 2009; Breiter et al., 2013) and it is important to establish whether diffusive processes can give rise to similar phenomena. Interestingly, we can find no study into Al/Ti from magmatic quartz (particularly among granitoids which may undergo different cooling rates) that mentions diffusion or even considers it pertinent to trace element ratios. It is also worth noting that, while we see no obvious thermodynamic connection between Al/Ti and extent of crystal fractionation, there might be an explanation rooted in diffusion. To investigate this phenomenon, simulations were carried out with diffusion models on a quartz sphere with an initial Al/Ti = 1 throughout the grain that contains eight domains of equal width where the initial concentration of both elements is at a ratio of 2:1 in adjacent domains. As indicated by results presented in Figure 9, the subtle differences in Ti and Al lattice diffusion can give rise to Al/Ti fractionation at the locus of a concentration interface. This type of diffusion-driven process is, however, unlikely to give rise to Al:Ti observed within magmatic quartz at the grain scale (e.g., >100 μm), such that the Al/Ti

fractionation hypotheses of Müller et al. (2002), Jacamon and Larsen (2009) and Breiter et al. (2013) is sound from a lattice diffusion perspective. This being the case, the subtle difference in Al and Ti diffusivity illustrated in Figure 9 also indicate that it is possible to monitor diffusion driven fractionation of Al/Ti at scales of 1-10s of microns (specifically at magmatic temperatures and cooling rates). This is to say that studies into temperature-time paths that involve Ti lattice diffusion models across concentration domains within volcanic quartz (typically imaged by cathodoluminescence; e.g., Matthews et al., 2012) may benefit from including Al in their calculations. The addition of Al to these types of diffusion calculations would be fortuitous as Al is generally the most abundant impurity within magmatic quartz. It is important to stress that as Al is not generally considered a cathodoluminesence activator in quartz (with Ti being the dominant activator) it first important to establish/consider whether an observed concentration interface within quartz is common for the two elements.

Conclusions

The diffusion results presented here clearly demonstrate that Al diffusivity is limited in magmatic quartz and is highly unlikely to significantly modify any zoned quartz that crystallized at low temperature conditions (<650 °C), even at very slow cooling rates seen in nature. This in turn tends to suggest that Al concentration likely preserves information pertaining to the original crystallization environment and the initial zonation observed in a majority of quartz grains that are not subsequently modified by other processes (e.g., dissolution-precipitation, dynamic recrystallization, etc). The subtly different Arrhenius parameters for Al and Ti also suggests the two elements are unlikely to diffusively

fractionate at the grain scale (e.g., >100 μm), making Al/Ti an accurate record of crystallization conditions. Modeling results presented in this study do, however, demonstrate that small-scale variations (e.g., at or below the 1-10 μm) may prove useful in future studies of magmatic time-temperature paths.

Acknowledgements:

This work was supported by the NASA Astrobiology Institute grant no. NNA09DA80A to RPI. NDT would like to thank Jay Thomas, Dustin Trail and Mike Ackerson for their on-going assistance during the development of this manuscript.

References

Ackerson, M.R., Tailby, N.D., and Watson, E.B. (2015) Trace elements in quartz shed light on sediment provenance. Geochemistry, Geophysics, Geosystems, 16, 1894-1904.

Allan, M.M., and Yardley, B.W.D. (2007) Tracking meteoric infiltration into magmatic-hydrothermal system: A cahthodoluminescence, oxygen isotope and trace element study of quartz from Mt. Leyshon, Australia. Chemical Geology, 240, 343-360.

Botis, S.M., and Pan, Y. (2009) Theoretical calculations of $[AlO_4/M^+]^0$ defects in quartz and crystal-chemical controls on the uptake of Al. Mineralogical Magazine, 73, 537-550.

Breiter, K., and Müller, A. (2009) Evolution of rare-metal granitic magmas documented by quartz chemistry. European Journal of Mineralogy, 21, 335-346.

Breiter, K., Ackerman, L., Svojtka, M., and Müller, A. (2013) Behavior of trace elements in quartz from plutons of different geochemical signature: A case study from the Bohemian Massif, Czech Republic. Lithos, 175-176, 54-67.

Cherniak, D.J. (1995) Sr and Nd diffusion in titanite. Chemical Geology, 125, 219-232.

Cherniak, D.J. (2010) Diffusion in Quartz, Melilite, Silicate Perovskite, and Mullite. Reviews in Mineralogy and Geochemistry, 72, 735-756.

Cherniak D.J., and Lanford W.A. (2001) Nuclear Reaction Analysis. In: Non-Destructive Elemental Analysis. Alfassi Z. (ed.) Blackwell Science, pp 308-338.

Cherniak, D.J., and Watson, E.B. (1992) A study of strontium diffusion in plagioclase using Rutherford Backscattering Spectroscopy. Geochimica et Cosmochimica Acta, 58, 5179-5190.

Compston, W., and Pidgeon, R. T. (1986) Jack Hills, evidence of more very old detrital zircons in Western Australia. Nature, 321, 766-769.

Davis, J.W., Coleman, D.S., Gracely, J.T., Gaschnig, R., and Steam, M. (2012) Magma accumulation rates and thermal histories of plutons of the Sierra Nevada batholiths, CA. Contributions to Mineralogy and Petrology, 163, 449-465.

Dohmen, R., Kasemann, S.A., Coogan, L., Chakraborty, S. (2010). Diffusion of Li in olivine. Part 1: Experimental observations and multi species diffusion model. Geochimica et Cosmochimica Acta. 74, 274-292.

Götze, J. (2009) Chemistry, textures and physical properties of quartz – geological interpretation and technical application. Mineralogical Magazine, 73, 645-671.

Götze, J., Plötze, M., Graupner, T., Hallbauer, D.K., and Bray, C. (2004) Trace element incorporation into quartz: a combined study by ICP-MS, electron spin resonance, cathodoluminescence, capillary ion analysis and gas chromatography. Geochimica et Cosmochimica Acta, 68, 3741-3759.

Jacamon, F., and Larsen, R.B. (2009) Trace element evolution of quartz in the charnockitic Kleivan granite, SW-Norway: The Ge/Ti ratio of quartz as an index of igneous differentiation. Lithos, 107, 281-291.

Jourdan, A.-L., Vennemann, T.W., Mullis, J., and Ramseyer, K. (2009) Oxygen isotope sector zoning in natural hydrothermal quartz. Mineralogical Magazine. 73, 615-632.

Joyce, A.S. (1973) Application of cluster analysis to detection of subtle variation in a granitic intrusion. Chemical Geology, 11, 297-306.

Lanzillo, N.A., Watson, E.B. Thomas, J.B., Nayak, S.K., and Curioni, A. (2014) Near-surface controls on the composition of growing crystals: Car-Parrinello molecular dynamics (CPMD) simulations of Ti energetics and diffusion in alpha quartz. Geochimica et Cosmochimica Acta, 131, 33-46.

Larsen, R.B., Henderson, I., Ihlen, P.M., and Jacamon, F. (2004) Distribution and petrogenetic behavior of trace elements in granitic pegmatite quartz from South Norway. Contributions to Mineralogy and Petrology, 147, 615-628.

Müller, A., Kronz, A., and Breiter, K. (2002) Trace elements and growth patterns in quartz: a fingerprint of the evolution of the subvolcanic Podlesí Granite System (Krušné hory Mts., Czech Republic). Bulletin of the Czech Geological Survey, 77, 135-145.

Müller, A., Ihlen, P.M., and Kronz, A. (2008) Quartz chemistry in polygeneration Sveconorwegian pegmatites, Froland, Norway. European Journal of Mineralogy, 20, 447-463.

Müller, A., Wiedenbeck, M., van den Kerkhof, A.M., Kronz, A., and Simon, K. (2003) Trace elements in quartz – a combined electron microprobe, secondary ion mass spectrometry, laser-ablation ICPMS, and cathodoluminescence study, European Journal of Mineralogy, 15, 747-763.

Landtwing, M., and Pettke, T. (2005) Relationships between SEM-cathodoluminescence response and trace-element composition of hydrothermal vein quartz. American Mineralogist, 90, 122-131.

Pankrath, R., and Flörke, O.W. (1994) Kinetics of Al-Si exchange in low and high quartz: calculation of Al diffusion coefficients. European Journal of Mineralogy, 6, 435-457.

Roddick, J.C., and Compston, W. (1976) Radiometric evidence for the age of emplacement and cooling of the Murrumbidgee Batholith. Journal of the Geological Society of Australia, 23, 223-233.

Rusk, B.G., Lowers, H.A., and Reed, M.H. (2008) Trace elements in hydothermal quartz: Relationships with cathodoluminescence and insights into vein formation. Geology, 36, 547-550.

Tailby, N.D., Thomas, J.B., and Watson, E.B. (2010) Trace elements in quartz: experimental constraints on Al, Ti, Fe and P saturation. Geochimica et Cosmochima Acta, 74, A1020.

Tetley, N.W. (1979) Geochronology by the $^{40}Ar/^{39}Ar$ technique using HIFAR reactor, 610p. Ph.D. thesis, Australian National University.

Thomas, J., Watson, E.B., Spear, F.S., Shemella, P.T., Nayak, S.K., and Lanzirotti, A. (2010) TitaniQ under pressure: the effect of pressure and temperature on the solubility of Ti in quartz. Contributions to Mineralogy and Petrology, 160, 743-759.

Verhoogen J. (1952) Ionic diffusion and electrical conductivity in quartz. American Mineralogist, 37, 637-655.

Wark, D.A., and Watson, E.B. (2006) TitaniQ: a titanium-in-quartz geothermometer. Contributions to Mineralogy and Petrology, 152, 743-754.

Watson, E.B., and Cherniak, D.J. (2013) Simple equations for diffusion in response to heating. Chemical Geology, 335, 93-104.

Watson, E.B., and Dohmen, R. (2010) Non-traditional and emerging methods for diffusion measurements. In Y. Zhang and D. Cherniak, Eds, Diffusion in Minerals and Melts, 72, p.61-105. Reviews in Mineralogy and Geochemistry, Mineralogical Society of America, Chantilly, Virginia.

Watson, E.B., and Müller, T. (2009) Non-equilibrium isotopic and elemental fractionation during diffusion-controlled crystal growth under static and dynamic conditions. Chemical Geology, 267, 111-124.

Watson, E.B., Wanser, K.H., and Farley, K.A. (2010) Anisotropic diffusion in a finite cylinder, with geochemical applications. Geochimica et Cosmochimica Acta, 74, 614-633.

Wiebe, R.A., Wark, D.A., and Hawkins, D.P. (2007) Insights from quartz cathodoluminescence zoning into crystallization of the Vinalhaven granite, coastal Maine. Contributions to Mineralogy and Petrology, 154, 439-453.

Ziegler, J.F., Biersack, J.P. (2006) The stopping and range of ions in matter. Computer code SRIM 2006, http://www.srim.org.

Table 1: Experimental run details for diffusion experiments

									measured		*fit*	
Run #	**Quartz type**	**Orientation**	**Source**	**Time (sec)**	**Temp**	**D**	**error**	**logD**	**C_0 (ppmw)**	**C_0 std error**	**C_0 (ppmw)**	**C_0 std error**
Al measurements												
AlQ-d-14	Syn	⊥C	Kyanite	2.33E+06	708	2.85E-22	1.90E-23	-21.5	2116	312	1959	79
AlQ-d-15	Syn	⊥C	Spod*	2.14E+06	732	2.17E-21	3.37E-22	-20.7	3601	403	3262	220
AlQ-d-16	Syn	⊥C	Kspar	2.06E+06	763	1.43E-21	2.21E-22	-20.8	512	147	469	50
AlQ-d-07	Syn	⊥C	Spod	5.18E+06	767*	6.50E-22	1.28E-22	-21.2	2182	287	2286	255
AlQ-d-21a	Syn	⊥C	Spod*	1.69E+05	795†	1.62E-20	3.56E-21	-19.8	1016	203	1063	130
AlQ-d-21b	Syn	⊥C	Spod*	4.29E+06	795†	1.54E-20	1.09E-21	-19.8	5055	453	5192	118
AlQ-d-21c	Syn	⊥C	Spod*	6.48E+05	795†	1.02E-19	2.41E-20	-19.0	2627	274	2589	425
AlQ-d-21d	Syn	⊥C	Spod*	1.55E+06	795†	1.49E-20	1.55E-21	-19.8	3793	338	3489	163
AlQ-d-27	Syn	⊥C	Spod*	8.64E+05	830	1.36E-21	1.43E-22	-20.9	4135	286	4344	166
AlQ-d-03	Syn	⊥C	Kspar	7.78E+05	888	1.75E-20	2.71E-21	-19.8	1671	275	1659	76
AlQ-d-18	Syn	⊥C	Kspar	1.67E+05	933	6.77E-20	1.06E-20	-19.2	1851	296	1518	87
AlQ-d-08	Syn	‖C	Spod	3.46E+06	700	3.87E-22	6.10E-23	-21.4	1305	242	1290	104
AlQ-d-17	Syn	‖C	Spod	1.91E+06	750	5.11E-21	1.59E-21	-20.3	1141	316	806	108
AlQ-d-10	Syn	‖C	Spod	1.21E+06	807	6.91E-21	1.66E-21	-20.2	675	174	577	47
AlQ-d-20	Syn	‖C	Kspar	6.86E+05	860	9.57E-20	6.72E-20	-19.0	903	168	458	68
AlQ-d-26	Syn	‖C	Kspar	1.67E+05	900	8.97E-21	1.38E-21	-20.0	2983	723	4427	484
AlQ-d-06	Syn	‖C	Spod	7.56E+04	950	5.11E-20	1.39E-20	-19.3	4297	614	4616	748
AlQ-d-04	Syn	‖C	Spod	7.56E+04	950	9.56E-20	2.16E-20	-19.0	1843	402	1577	175
AlQ-nd-01	Herk	‖C	Spod*	5.11E+05	758	2.74E-21	3.93E-22	-20.6	483	58	492	39
AlQ-nd-02	Ark	‖C	Spod*	1.30E+06	815	1.27E-21	1.76E-22	-20.9	1732	265	1863	304
AlQ-nd-04	Ark	‖C	Spod*	5.18E+05	818	3.78E-21	2.83E-22	-20.4	663	65	601	20
Li experiments												

AlQ-d-21d	Syn	⊥C	Spod*	1.55E+06	795	2.65E-20	4.14E-21	-19.6	819	78	1037	58
AlQ-d-21b	Syn	⊥C	Spod*	4.29E+06	795	4.42E-20	9.15E-21	-19.4	2576	163	2236	84
Al measurements from literature												
	P & F	‖C		1.73E+05	400	6.1E-27	1.30E-27	-26.2	2985			
	P & F	‖C		?	525	2.1E-24	5.00E-25	-23.7	2986			
	P & F	⊥C		1.73E+05	400	9.20E-27	1.80E-27	-26.0	2988			
	P & F	⊥C		?	525	3.10E-24	8.00E-25	-23.5	2989			

*indicates natural mineral diffusant source (Spod = Spodumene, Kspar = $KAlSi_3O_8$)

†indicates time-series experiment (i.e., constant temperature, different durations)

P & F represents data published by Pankrath and Flörke (1994)

C_0 (measured) corresponds to surface concentration as determined by NRA analysis, C_0 (fit) corresponds to the surface concentration calculated from the diffusion profile fit.

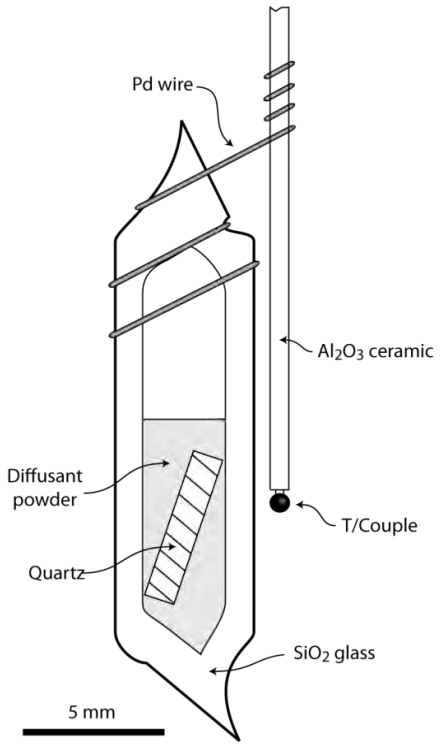

Figure 1: Experimental setup for semi-infinite source diffusion experiment.

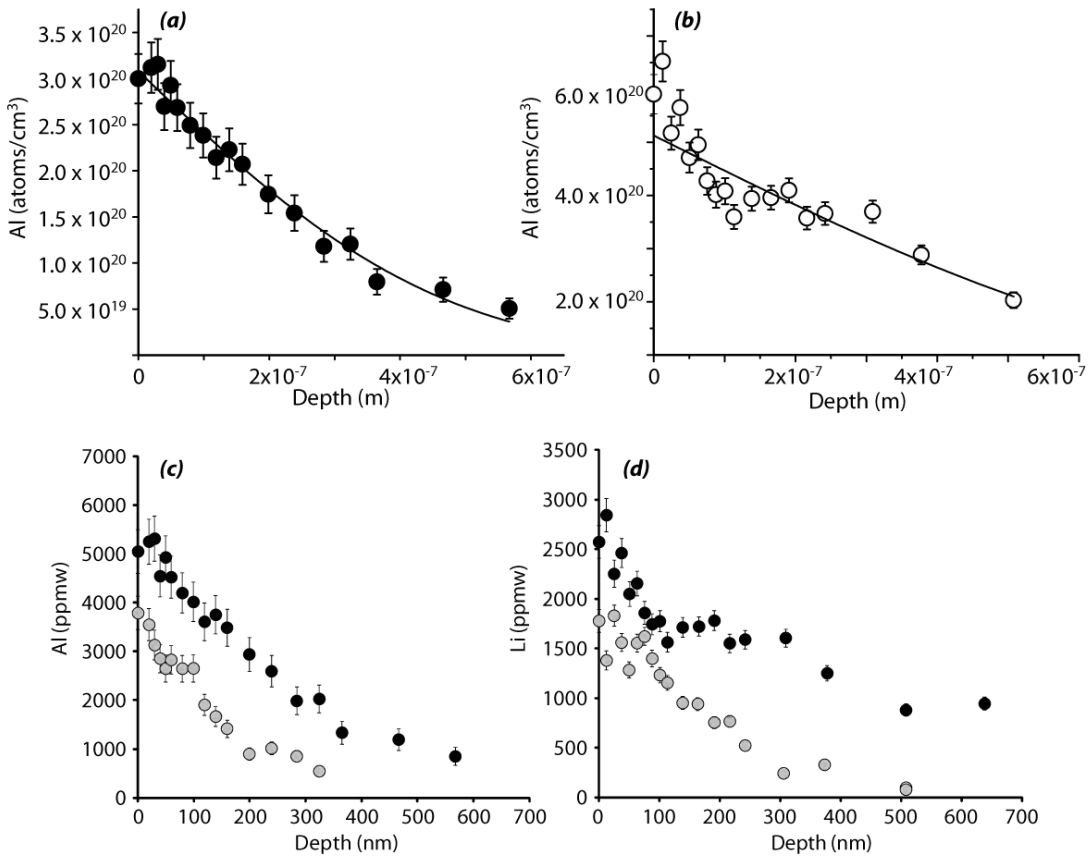

Figure 2: Representative diffusion diffusion profiles from isothermal experiments carried out 795 ˚C over different timescales (e.g., time-series experiments). Grey circles represent an ~18 day experiment, and solid circles represent an ~49 day experiment. Note that surface concentration remains at similar values despite different experiment durations (indicative of a semi-infinite source at constant surface concentration). For each data point the error varies depending on γ yield at the energy of interest and background in this energy region. (a) Reduced Al diffusion data employing a semi-infinite source at constant concentration fit [where, $(C(x,t) = C_0 \mathrm{erfc}(x/(4Dt)^{\frac{1}{2}})$] for ~49 day experiment. (b) Diffusion profiles from ~8 day/795 ˚C diffusion experiment with open diamonds = Li

data and solid circles = Al data (units now in ppmw and nanometers). Note the similarity of Li and Al profiles. (c) Al diffusion profiles from 795 ˚C time series experiments, and (d) Li diffusion profiles from the same experiments shown in Figure 2c. Where absent error bars are smaller than symbols.

.

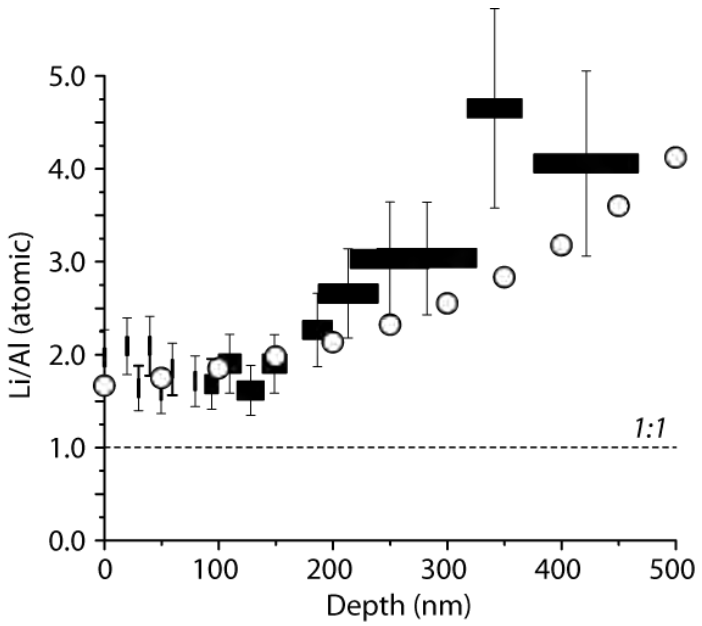

Figure 3: Measured Li/Al (solid rectangles) and calculated Li/Al from diffusion profile fits for Li and Al in the ~49 day spodumene-quartz experiment (same data as Figure 2a and 2b). Note the large y-axis (depth) variation at depth is due to NRA measurements being obtained at different depths within the host quartz crystal (rather than representing intrinsic analytical uncertainty). 1:1 line expected for $LiAlO_2$-type substitution is represented by the dashed line.

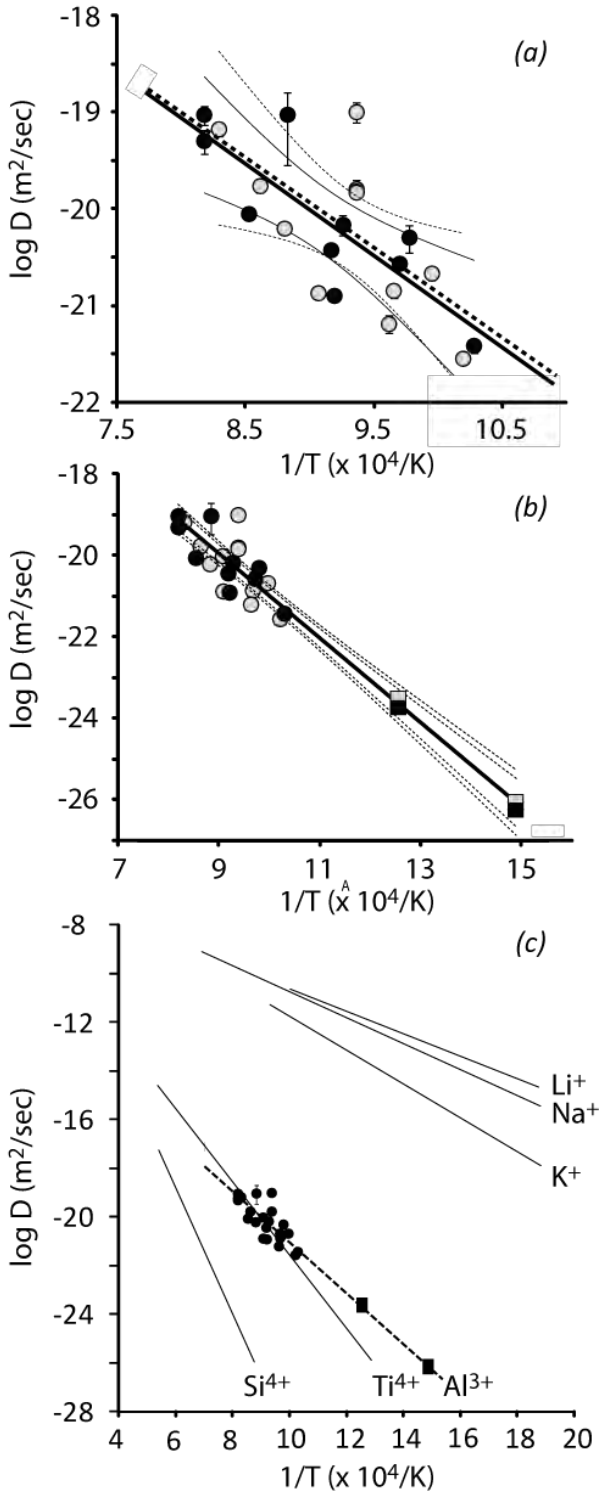

Figure 4: Arrhenius parameters for Al^{3+} and other cations in quartz. (a) Arrhenius relations for Al-in-quartz from experiments presented in this study; solid symbols represent diffusion parallel to the c-axis, grey symbols represent diffusion perpendicular to the c-axis. Heavy line = linear regression to experiments perpendicular to the c-axis, heavy dashed line = linear regression to experiments parallel to the c-axis. The fine curves correspond to 95 % confidence interval for respective data sets; solid curve = perpendicular to c-axis, dashed curve = parallel to c-axis. (b) Arrhenius relations for all experiments presented here and data from Pankrath and Flörke (1994), symbols as in (a) with Pankrath and Florke data shown in squares (solid = parallel C, grey = perpendicular C). Solid heavy line represents linear regression to all data; dashed curves represent 95 % and 99 % confidence intervals for the fit. (c) Comparison of Arrhenius parameters of the dominant cations known to substitute in quartz, Al data and fit is shown with solid circles and dashed heavy line.

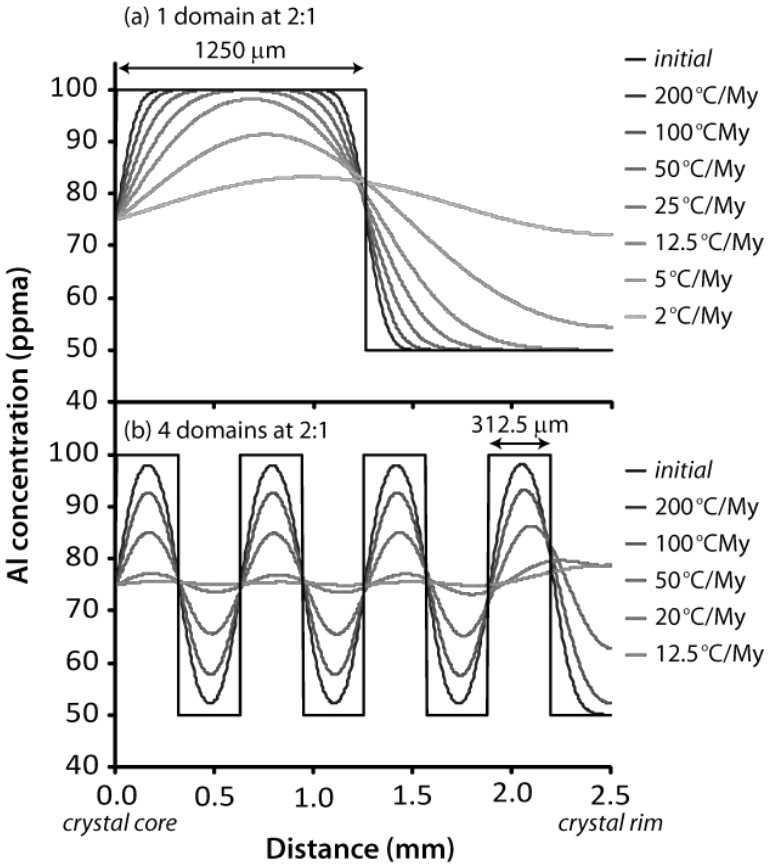

Figure 5: Simulated Al zonation in a magmatic grain over 700-500 ˚C cooling interval. (a) Simulated Al concentration (at an initial 2:1 for adjacent domains) over 2 domains in 2.5 mm radius crystal (e.g., zones of 625 µm constant concentration) at different cooling rates. (b) Simulated Al concentrations in grain of the same dimensions over 8 domains (e.g., zones of 312.5 µm constant concentration) at different cooling rates). Aluminum concentration at the surface of the spherical crystal (left side; r = 0) is held constant during the simulations at a value halfway between the initial minimum and maximum concentrations.

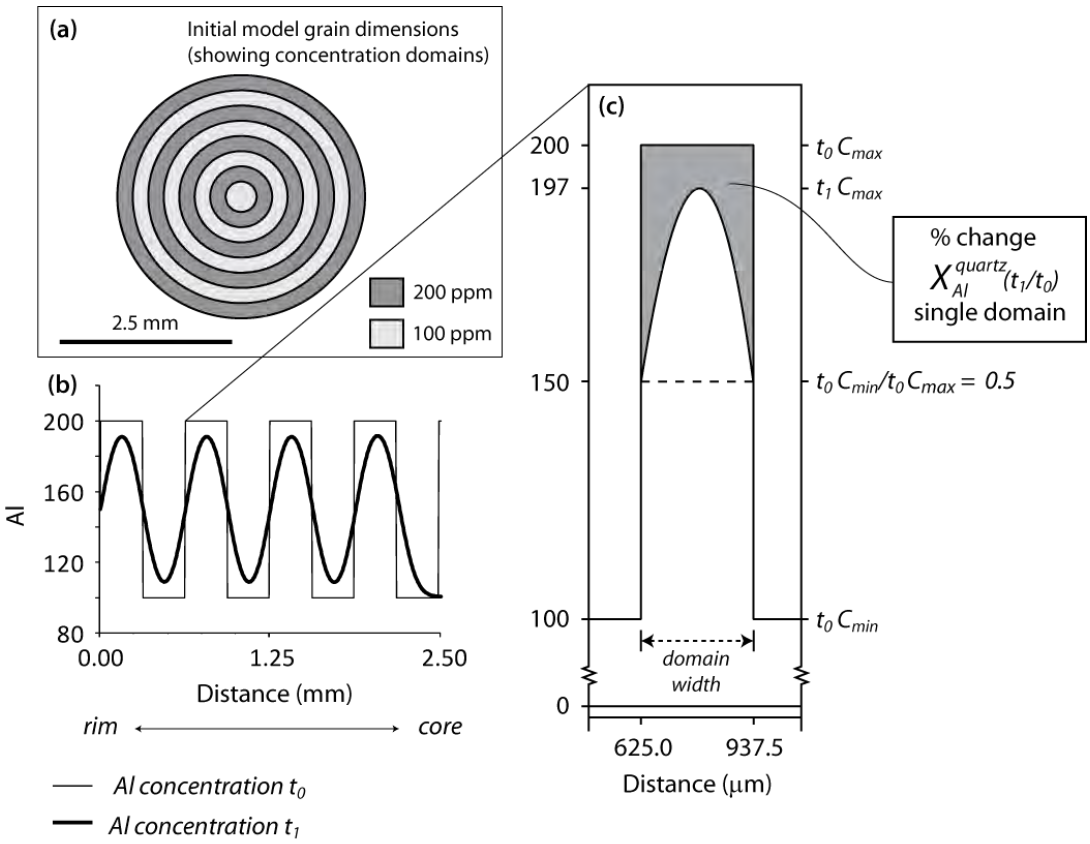

Figure 6: Simulated diffusion profile in quartz sphere containing 8 concentration domains (with initial Al concentration ratio of 2:1 for adjacent domains). Simulation was run at 20 ˚C/Myr over 10 Myr. (a) Simplified sketch of quartz concentration profile in quartz sphere, where dark domains indicate 200 ppm Al and light domains indicate 100 ppm Al. (b) Al concentration profile from rim to core of the quartz sphere at initial conditions (t_0 = dashed curve) and after the cooling cycle (t_1 = solid curve). (c) Concentration change within an individual domain (shaded region) from diffusive loss/gain from the domain. The integrated area of Al loss/gain can be used to calculate percent change (at 2:1 initial concentration variation, the maximum percent change is 25 %) that occurs within a domain as a function of time, cooling rate and length scales. Note that concentration change is calculated from the sum of nodes within an individual

domain, rather than modeled as a curve (such that accuracy is dependent on the number and spacing of nodes within a domain).

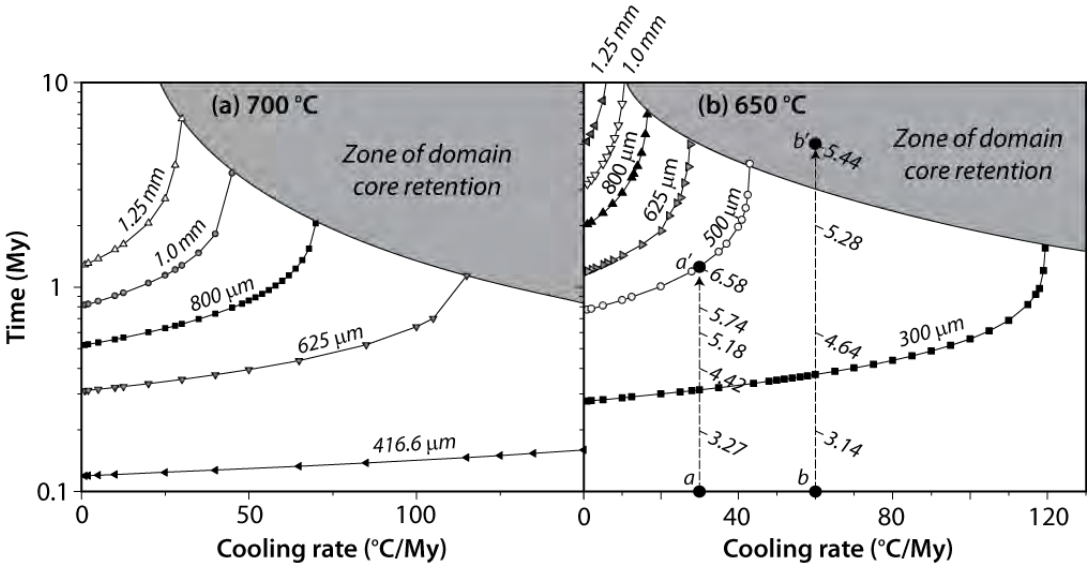

Figure 7: Simulation results for Al diffusion in a quartz sphere of 2.5 mm radius having alternating, concentric domains (bands) of high and low Al concentration (2:1 initial ratio). The radial widths of the domains modeled (312.5 to 1250 microns) are indicated on the figure. Results are shown for various cooling rates and cooling times; symbols are located at the point where the initial composition at the center of the high-concentration domain has just been compromised by diffusion. The shaded region corresponds to the time (My)-cooling rate (˚C/My) conditions where a spherical domain retains core concentration. Italic numerical values along a-a' and b-b' represent the percent domain change (as indicated in Figure 6c; where % change = $X_{Al}^{quartz}(t_1/t_0)$. It is worth noting

that the zone of retention will contract proportionately with increasing percent change. For discussion of vectors a-a' and b-b' see text.

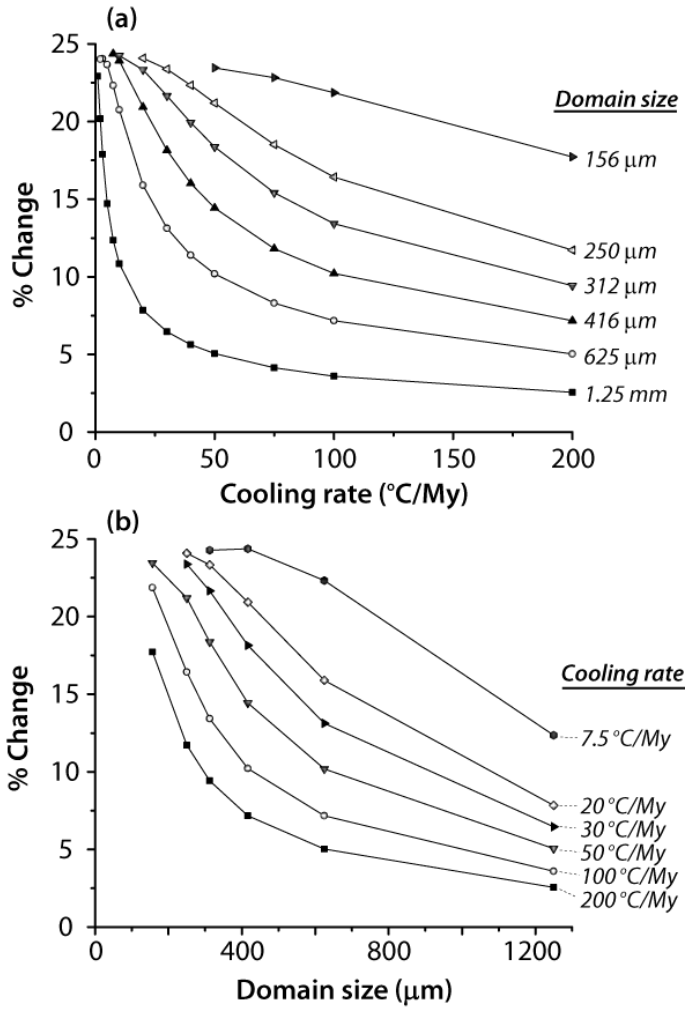

Figure 8: Modeled relationship between percentage change in Al concentration in domains of different width and different cooling rates, noting that all simulations were carried out on 2.5 mm radius quartz sphere with a an initial Al concentration ratio of 2:1 in adjacent domains. (a) Percent change in Al concentration in domains as a function of cooling rate; the curves illustrate the effects on domains of different widths. (b) Percent change in Al concentration for domains of different width in model spheres; the curves illustrate the effects of different constant cooling rates.

720

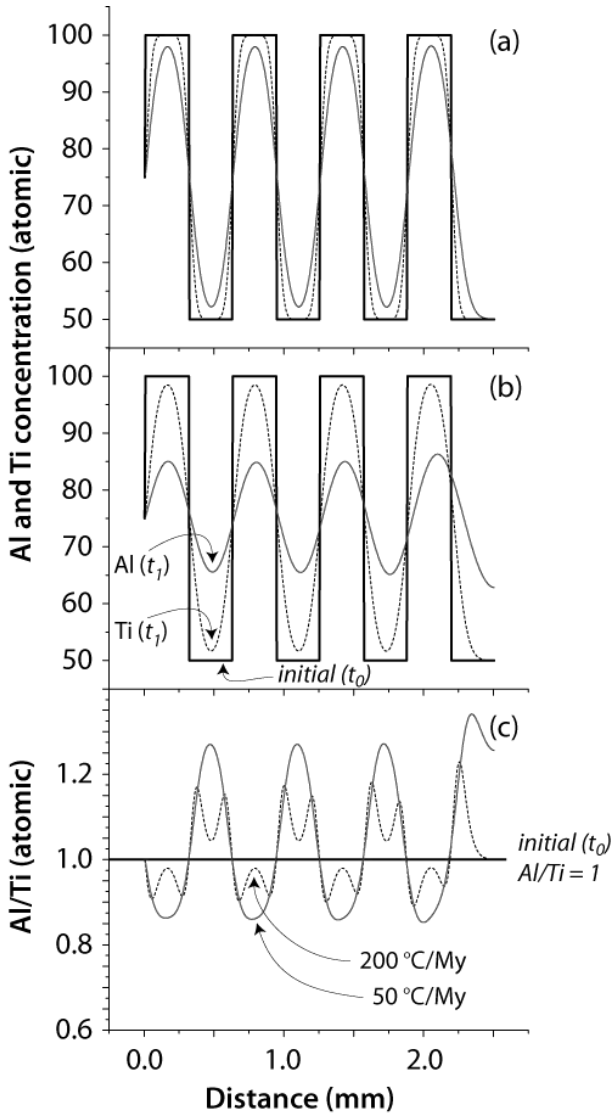

Figure 9: Simulation of diffusion-controlled Al/Ti fractionation for a 2.5 mm quartz sphere with initial concentration ratio Al/Ti = 1, a 2:1 initial concentration ratio in adjacent domains for both elements, and a cooling rate of 10 ˚C/My over 20 My. (a) Concentration profiles of Al and Ti at initial conditions (t_0) and diffusion-modified concentrations at t_1 (i.e., after 20 My at a cooling rate of 10 ˚C/My). (b) Al/Ti values at initial conditions (Al/Ti = 1) and diffusion-modified profile after 20 My of cooling.

Supplement 1

LA-ICP-MS analyses of polished quartz slabs was carried out on a Photon Machines 193 nm eximer laser system attached to a Bruker 820-MS quadrupole mass spectrometer. The analytical method involves an 80 um square, a fluence of 8.3 J/cm^2 and a pulse rate of 10 Hz. The mass scan includes ^{7}Li, ^{11}B, ^{23}Na, ^{24}Mg, ^{27}Al, ^{29}Si, ^{31}P, ^{39}K, ^{43}Ca, ^{47}Ti, ^{49}Ti, ^{57}Fe, ^{71}Ga, and ^{72}Ge. The analytical technique employs a He carrier gas (flow rate = 0.7 liters/minute) to transport the analyte from the ablation cell, was mixed with N_2 and transported to the plasma. Dwell time for individual masses was set at 10000 microseconds and the time-resolved spectra was collected over 80 seconds. A 20 second background counting period and ablation period of 30-40 seconds was used during each analysis. Standard glass NIST612 (Pearce et al., 2007) was used for calibration purposes while ^{29}Si was used as the internal standard.

This is a preprint, the final version is subject to change, of the American Mineralogist (MSA)
Cite as Authors (Year) Title. American Mineralogist, in press.
DOI: https://doi.org/10.2138/am-2018-5613

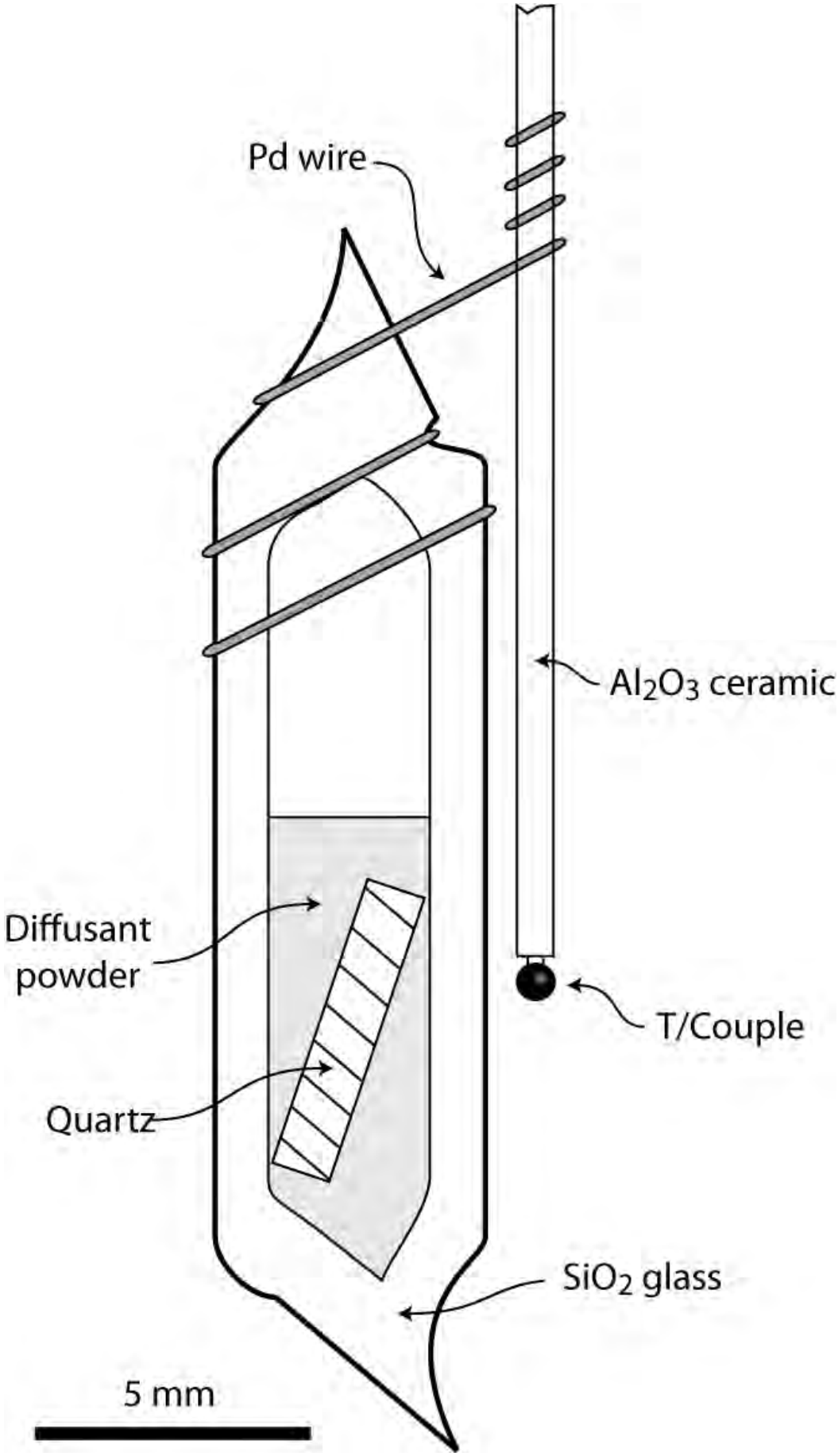

This is a preprint, the final version is subject to change, of the American Mineralogist (MSA)
Cite as Authors (Year) Title. American Mineralogist, in press.
DOI: https://doi.org/10.2138/am-2018-5613

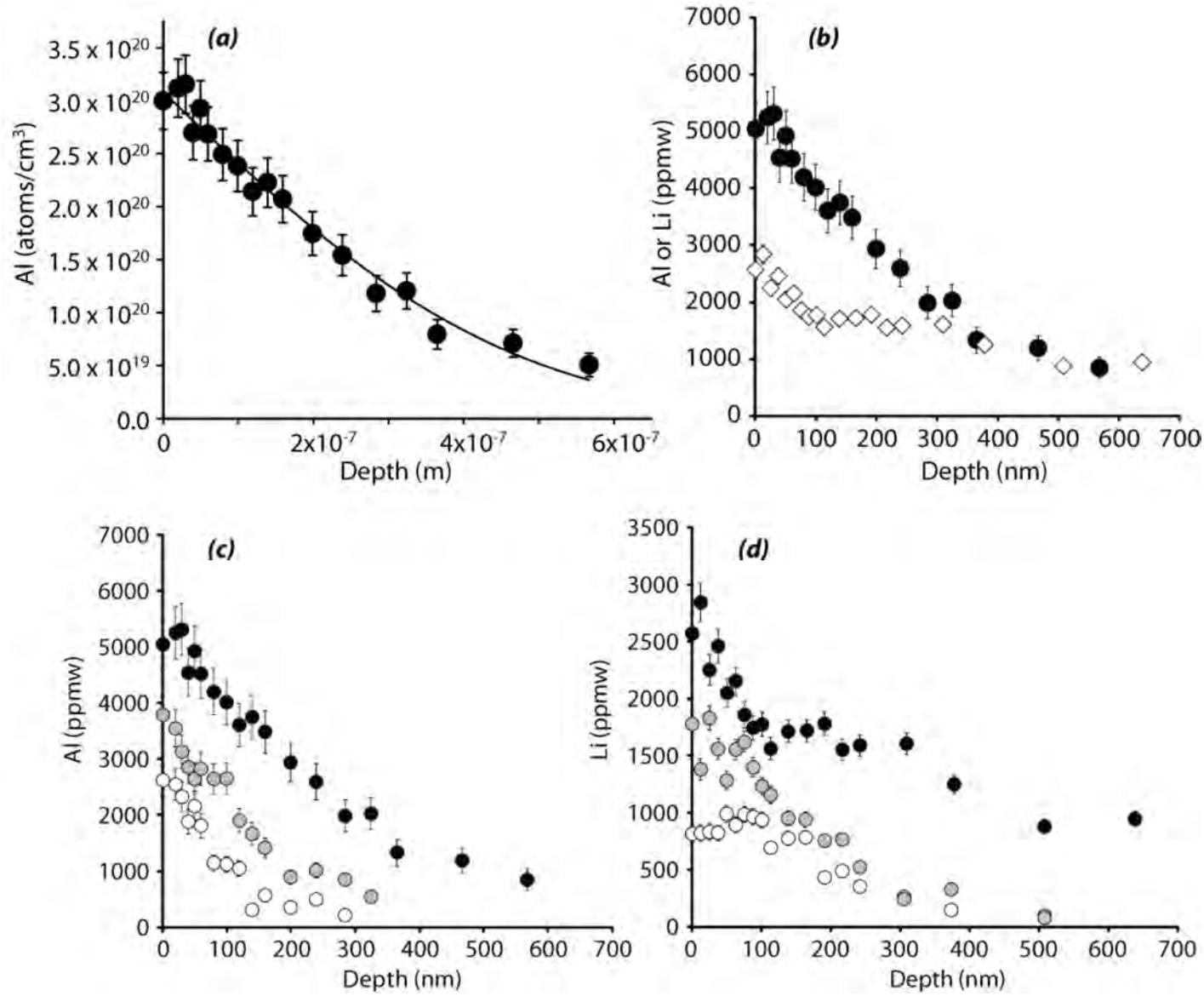

This is a preprint, the final version is subject to change, of the American Mineralogist (MSA)
Cite as Authors (Year) Title. American Mineralogist, in press.
DOI: https://doi.org/10.2138/am-2018-5613

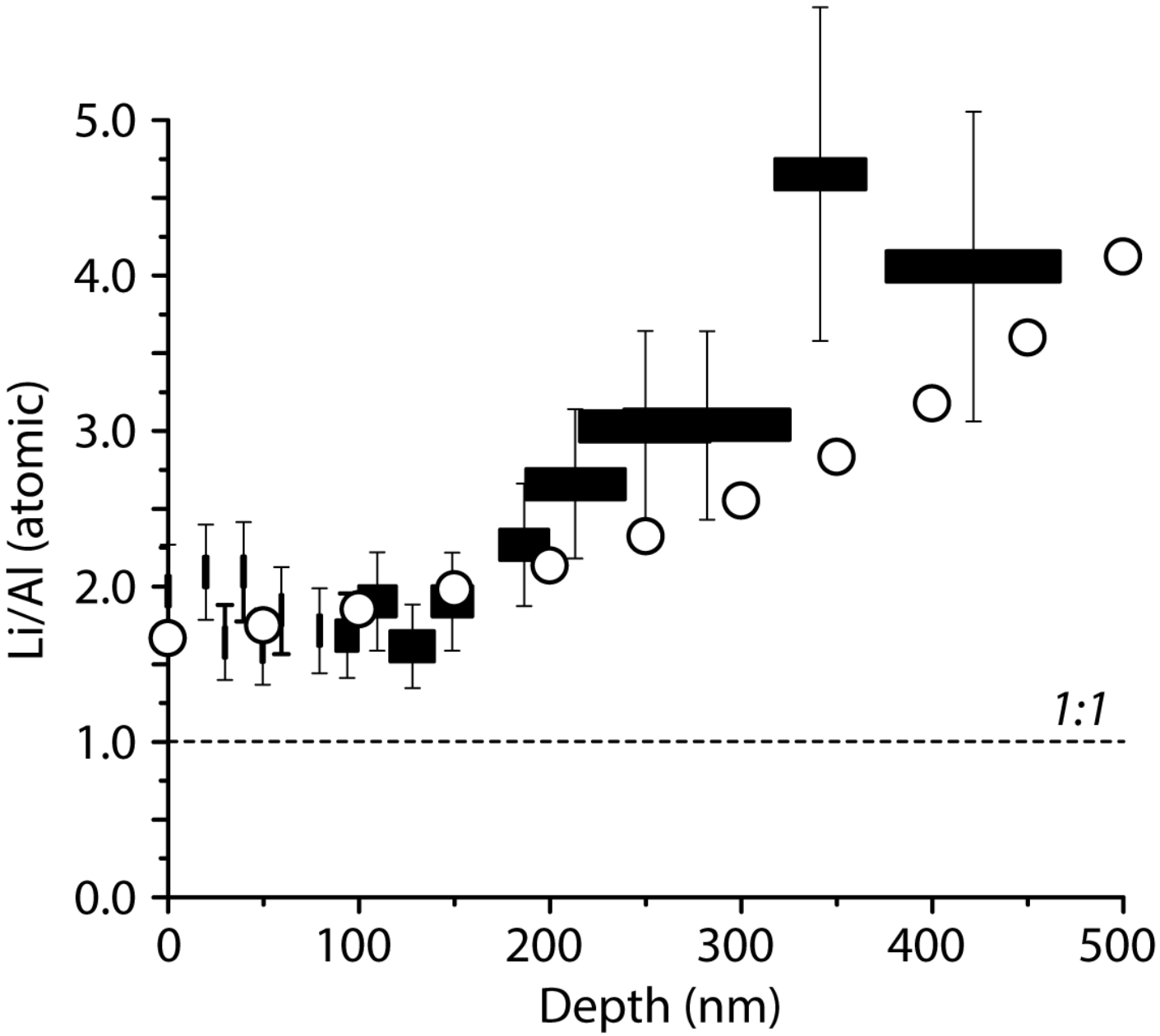

This is a preprint, the final version is subject to change, of the American Mineralogist (MSA)
Cite as Authors (Year) Title. American Mineralogist, in press.
DOI: https://doi.org/10.2138/am-2018-5613

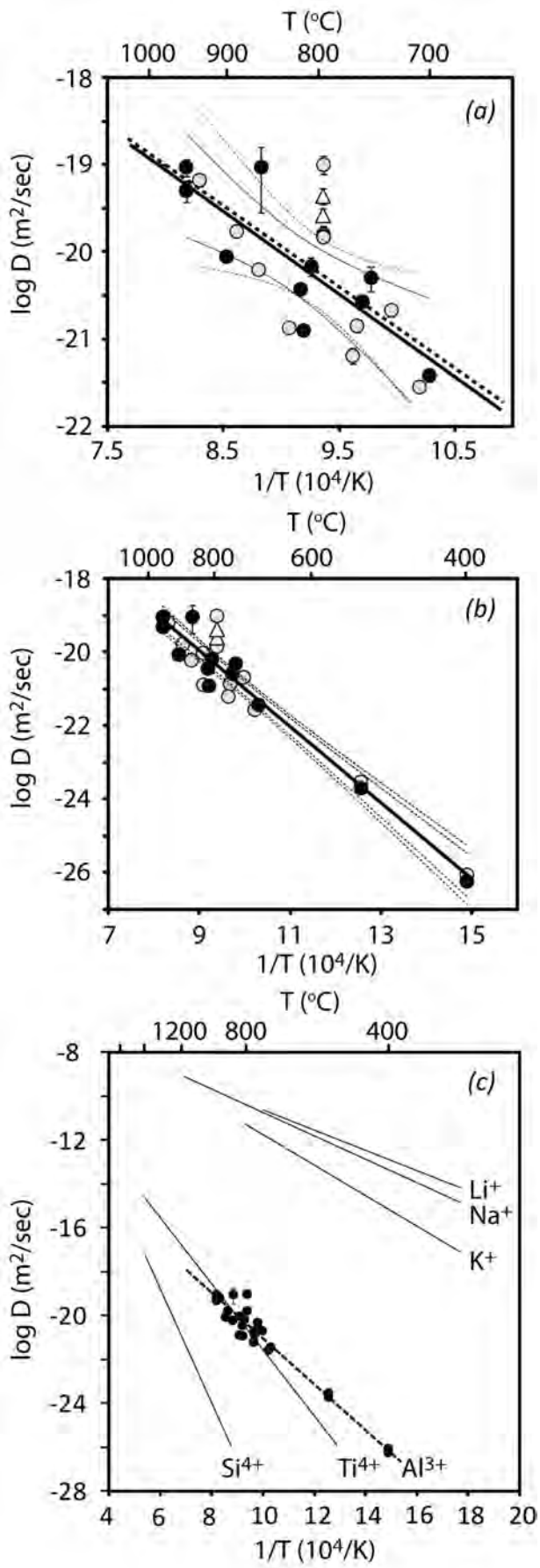

This is a preprint, the final version is subject to change, of the American Mineralogist (MSA)
Cite as Authors (Year) Title. American Mineralogist, in press.
DOI: https://doi.org/10.2138/am-2018-5613

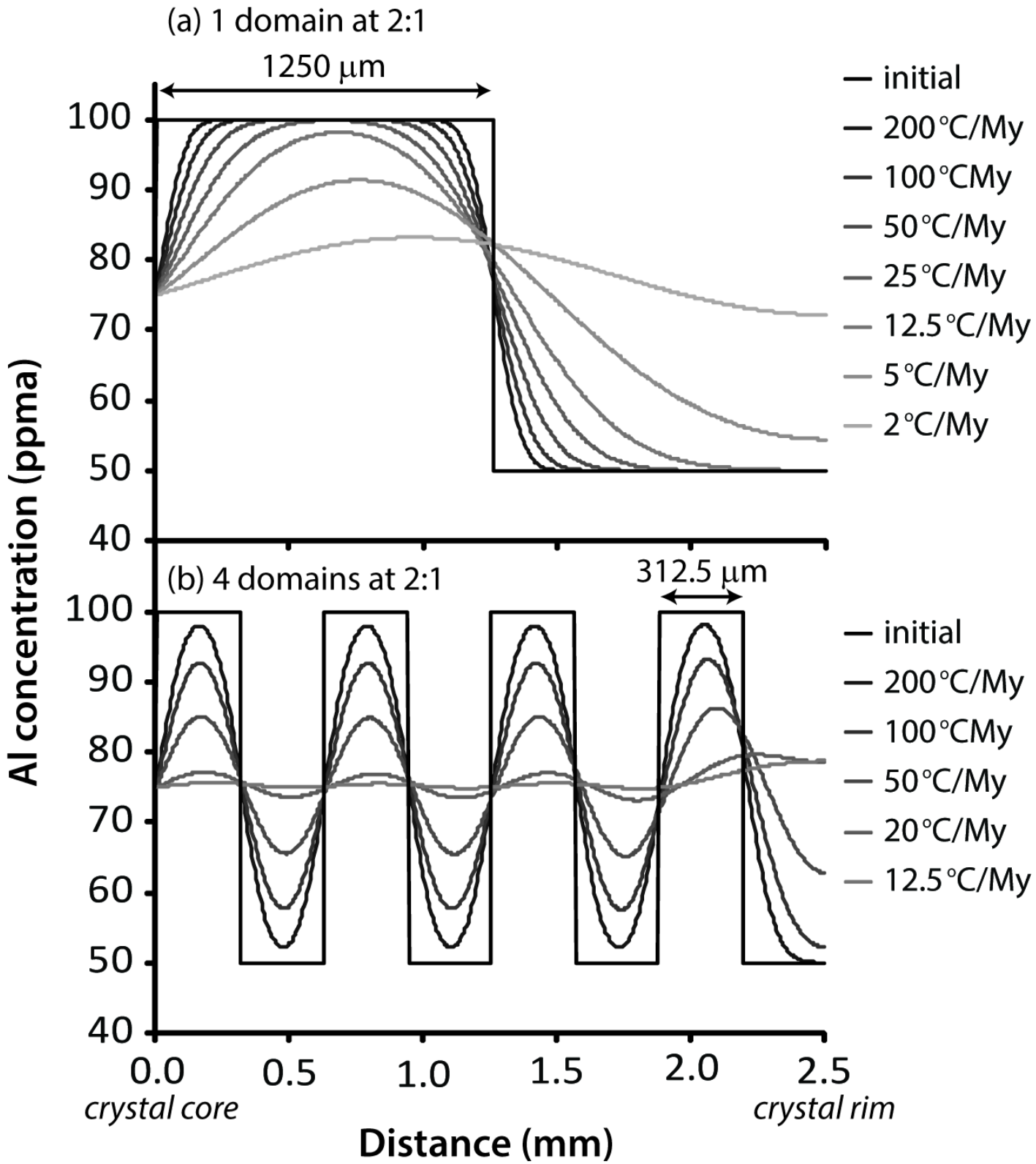

This is a preprint, the final version is subject to change, of the American Mineralogist (MSA)
Cite as Authors (Year) Title. American Mineralogist, in press.
DOI: https://doi.org/10.2138/am-2018-5613

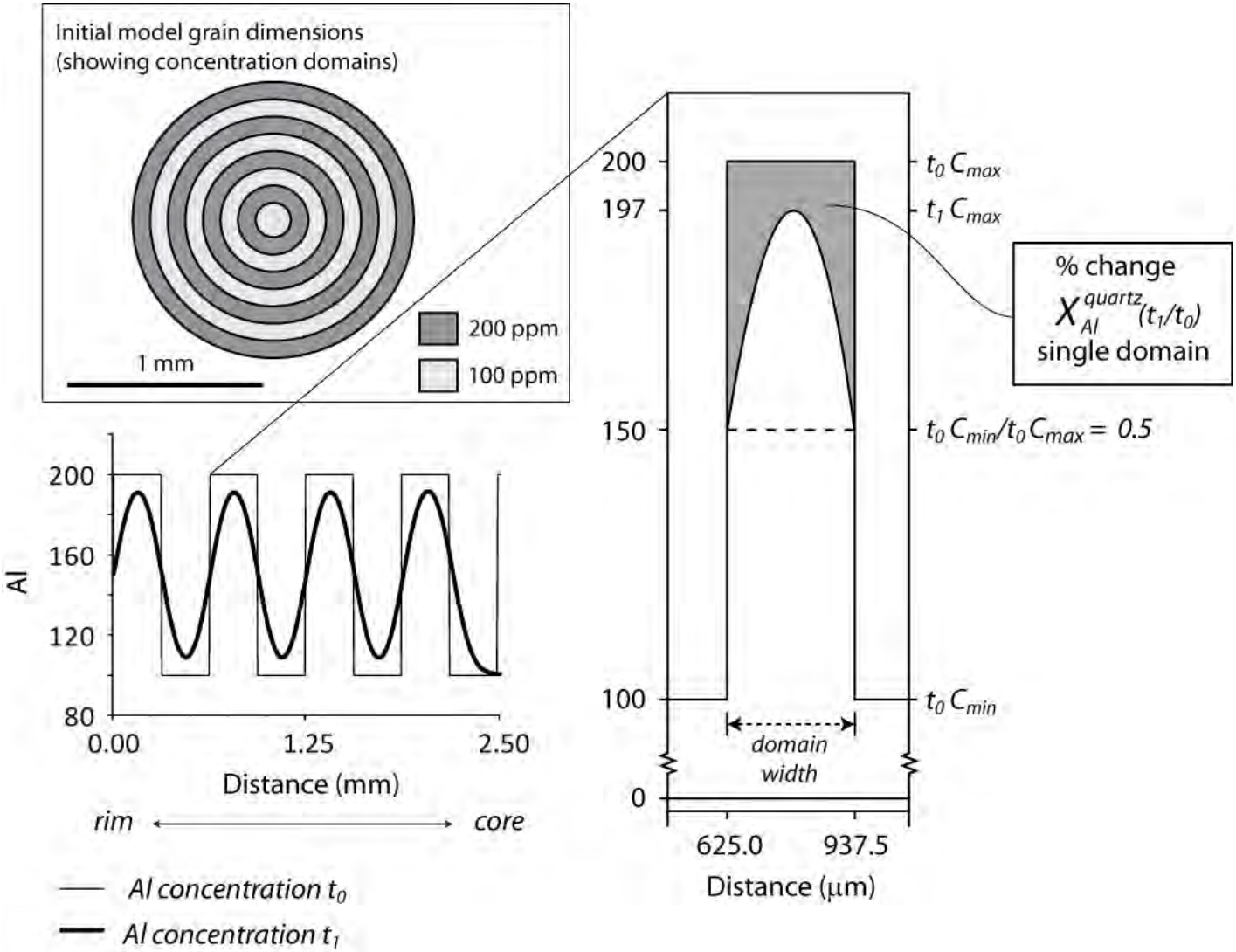

This is a preprint, the final version is subject to change, of the American Mineralogist (MSA)
Cite as Authors (Year) Title. American Mineralogist, in press.
DOI: https://doi.org/10.2138/am-2018-5613

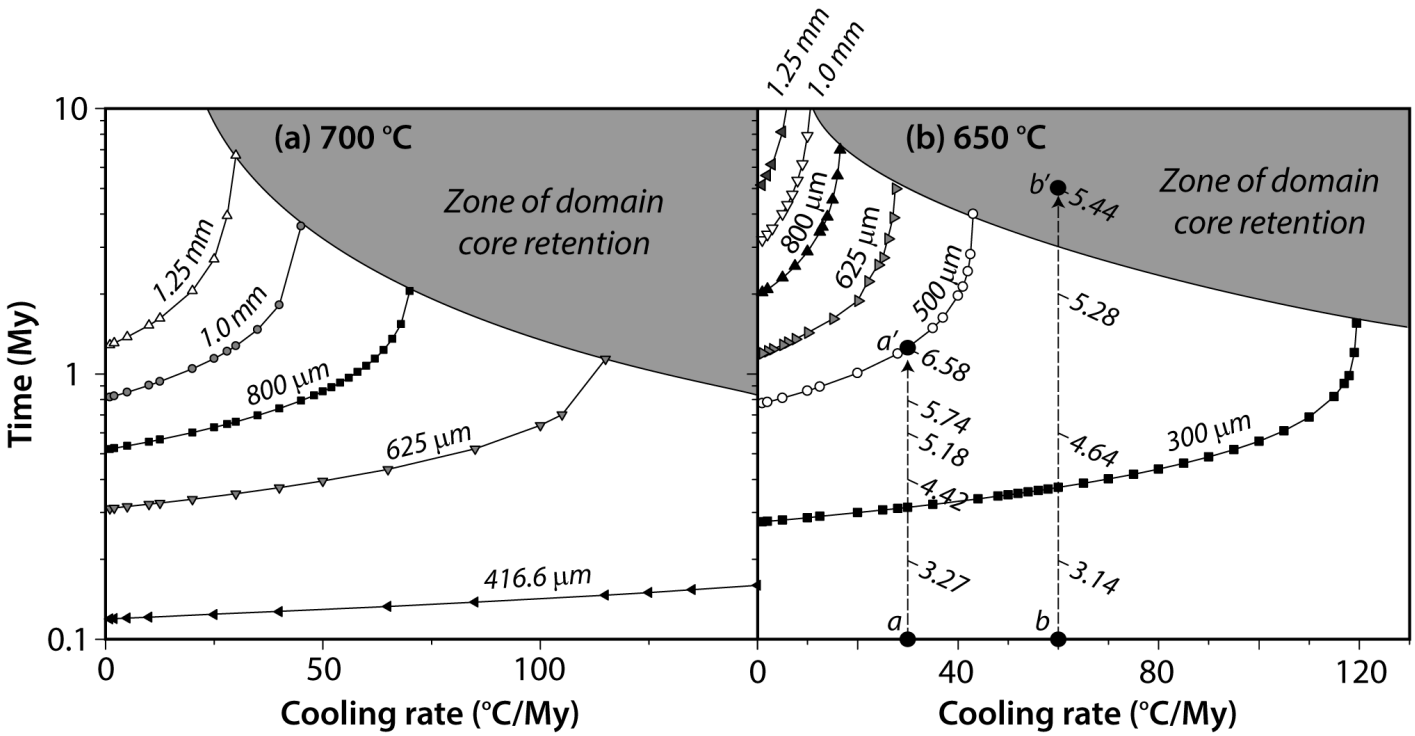

This is a preprint, the final version is subject to change, of the American Mineralogist (MSA)
Cite as Authors (Year) Title. American Mineralogist, in press.
DOI: https://doi.org/10.2138/am-2018-5613

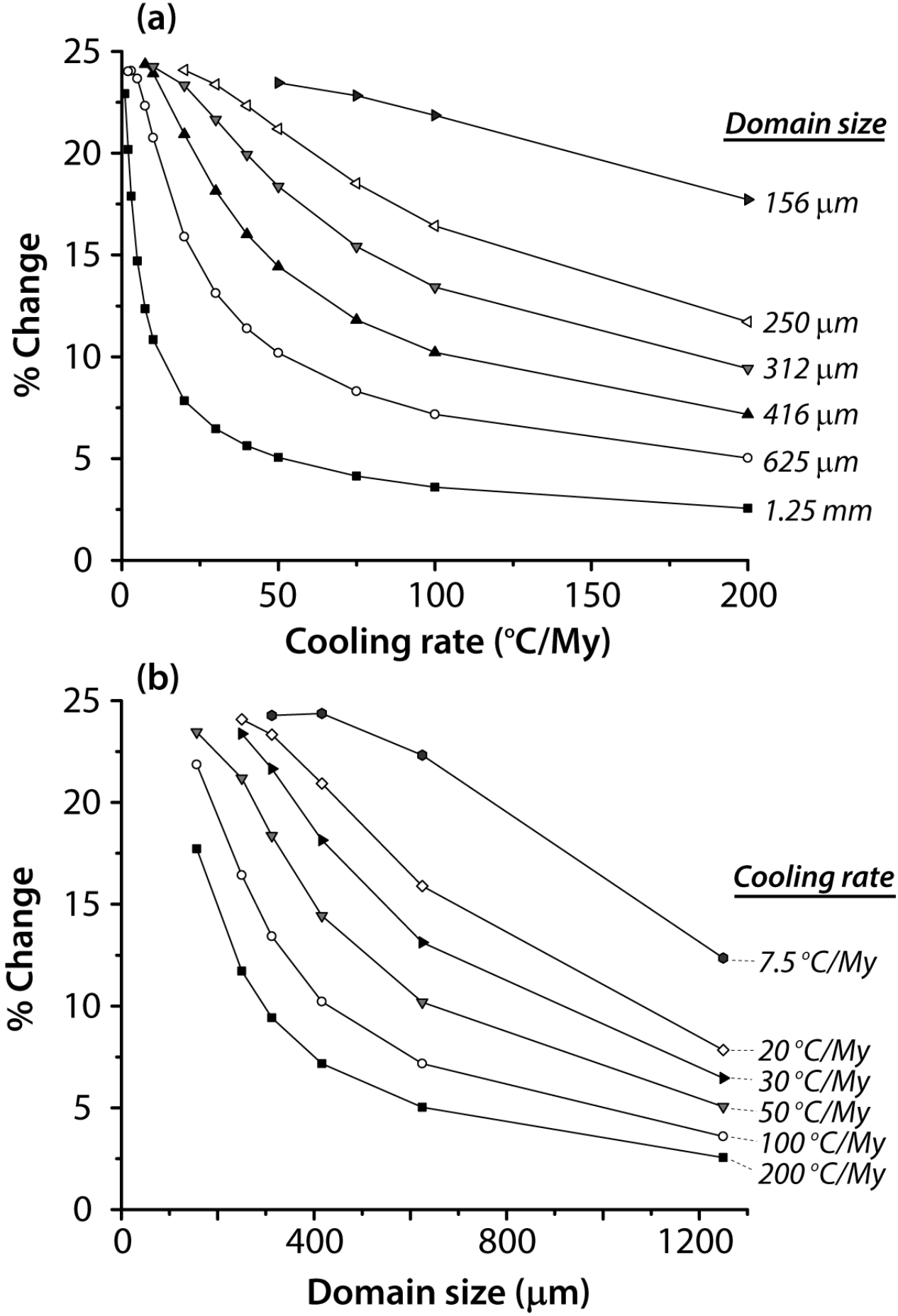

This is a preprint, the final version is subject to change, of the American Mineralogist (MSA)
Cite as Authors (Year) Title. American Mineralogist, in press.
DOI: https://doi.org/10.2138/am-2018-5613